Earth and Planetary Science Letters 289 (2010) 68–75

Contents lists available at ScienceDirect

Earth and Planetary Science Letters

journal homepage: www.elsevier.com/locate/epsl

Spin state of ferric iron in $MgSiO_3$ perovskite and its effect on elastic properties

Krystle Catalli [a,*], Sang-Heon Shim [a], Vitali B. Prakapenka [b], Jiyong Zhao [c], Wolfgang Sturhahn [c], Paul Chow [d], Yuming Xiao [d], Haozhe Liu [d], Hyunchae Cynn [e], William J. Evans [e]

[a] Department of Earth, Atmospheric and Planetary Sciences, Massachusetts Institute of Technology, Cambridge, MA 02139, USA
[b] GeoSoilEnviroCARS, University of Chicago, Argonne National Laboratory, Argonne, IL 60439, USA
[c] Sector 3, Advanced Photon Source, Argonne National Laboratory, Argonne, IL 60439, USA
[d] HPCAT, Advanced Photon Source, Argonne National Laboratory, Argonne, IL 60439, USA
[e] Lawrence Livermore National Laboratory, 7000 East Ave, Livermore, CA 94550, USA

ARTICLE INFO

Article history:
Received 2 February 2009
Received in revised form 9 October 2009
Accepted 21 October 2009

Editor: L. Stixrude

Keywords:
spin transition
ferric iron
lower mantle
silicate perovskite
elastic properties

ABSTRACT

Recent studies have indicated that a significant amount of iron in $MgSiO_3$ perovskite (Pv) is Fe^{3+} ($Fe^{3+}/\Sigma Fe = 10–60\%$) due to crystal chemistry effects at high pressure (P) and that Fe^{3+} is more likely than Fe^{2+} to undergo a high-spin (HS) to low-spin (LS) transition in Pv in the mantle. We have measured synchrotron Mössbauer spectroscopy (SMS), X-ray emission spectroscopy (XES), and X-ray diffraction (XRD) of Pv with all iron in Fe^{3+} in the laser-heated diamond-anvil cell to over 100 GPa. Fe^{3+} increases the anisotropy of the Pv unit cell, whereas Fe^{2+} decreases it. In Pv synthesized above 50 GPa, Fe^{3+} enters into both the dodecahedral (A) and octahedral (B) sites approximately equally, suggesting charge coupled substitution. Combining SMS and XES, we found that the LS population in the B site gradually increases with pressure up to 50–60 GPa where all Fe^{3+} in the B site becomes LS, while Fe^{3+} in the A site remains HS to at least 136 GPa. Fe^{3+} makes Pv more compressible than Mg-endmember below 50 GPa because of the gradual spin transition in the B site together with lattice compression. The completion of the spin transition at 50–60 GPa increases bulk modulus with no associated change in density. This elasticity change can be a useful seismic probe for investigating compositional heterogeneities associated with Fe^{3+}.

1. Introduction

Mg-silicate perovskite (Pv), with 5–10 mol% of Fe and Al, is the most abundant silicate mineral in the Earth, with a stability from 660-km depth to several hundred kilometers above the core–mantle boundary (Liu, 1976; Knittle and Jeanloz, 1987; Kesson et al., 1998; Shim et al., 2001b; Lee et al., 2004). Based on recent studies of iron in Pv, Fe^{3+} is emerging as an increasingly relevant component. Studies using starting materials containing only Fe^{2+} found that Pv in its stability field has a considerable amount of Fe^{3+}: $Fe^{3+}/\Sigma Fe \simeq 16\%$ without Al and $Fe^{3+}/\Sigma Fe \simeq 50–75\%$ with Al (McCammon, 1997). Several studies (Frost et al., 2004; Zhang and Oganov, 2006; Auzende et al., 2008) have shown that Fe^{2+} may disproportionate, creating free Fe metal, enriching Pv with Fe^{3+}. Frost et al. (2004) and McCammon (2005) argued that the significant amount of Fe^{3+} in Pv is not the result of the oxidation state of the lower mantle, which is expected to be reducing, but due to the crystal chemistry of Pv at high pressure.

Badro et al. (2004) reported a high-spin (HS) to low-spin (LS) transition in iron in Pv based on X-ray emission spectroscopy (XES), that occurred as a two step process. Li et al. (2004), however, found a gradual spin transition to occur both in Al-bearing and Al-free Pv which was still incomplete at 100 GPa based on XES. Based on a shift in the volume dependence of the relative center shift in synchrotron Mössbauer spectroscopy (SMS), Jackson et al. (2005) proposed a spin transition in the Fe^{3+}-like site completing near 70 GPa. McCammon et al. (2008) and Lin et al. (2008) observed an unusually high quadrupole splitting for Fe^{2+} and intermediate satellite peak intensity in XES, proposing a transition of Fe^{2+} from HS to intermediate spin.

In computational studies, Fe^{3+} was found to be in the LS state in the octahedral (hereafter B) site of Pv at all pressures relevant to the mantle and undergo a HS to LS transition in the dodecahedral (hereafter A) site at 60–150 GPa (Zhang and Oganov, 2006; Stackhouse et al., 2007). Stackhouse et al. (2007) showed that the transition pressure is highly dependent on the local iron configuration. Computational studies have found that Fe^{2+} remains HS throughout the mantle (Cohen et al., 1997; Li et al., 2005; Zhang and Oganov, 2006; Stackhouse et al., 2007). A more recent computational study (Umemoto et al., 2008) has shown that the spin transition of Fe^{2+} is possible but limited to specific configurations in Pv. In addition, computational studies do not support the stability of intermediate spin Fe^{2+} (Li et al., 2005; Zhang and Oganov, 2006; Bengtson et al., 2008; Bengtson et al., 2009). Therefore, Fe^{3+} may play an important role in the spin transition in Pv.

Fe^{3+} may also alter the properties of Pv. Increased Fe^{3+} in Pv has been found to significantly enhance the electrical conductivity (Xu

* Corresponding author.
E-mail address: krystle@mit.edu (K. Catalli).

0012-821X/$ – see front matter © 2009 Elsevier B.V. All rights reserved.
doi:10.1016/j.epsl.2009.10.029

et al., 1998). Also, Fe^{3+} may control the radiative conductivity of Pv in the lower mantle (Goncharov et al., 2008; Keppler et al., 2008). Although previous studies have investigated the equation of state of iron-bearing Pv (Knittle and Jeanloz, 1987; Andrault et al., 2001; Lundin et al., 2008), $Fe^{3+}/\Sigma Fe$ was not measured in those samples, and Mössbauer studies have shown a wide range of $Fe^{3+}/\Sigma Fe$ values even in the absence of Al (McCammon, 1997; Jackson et al., 2005).

There is a significant amount of ambiguity in interpreting Mössbauer results for Pv containing both Fe^{2+} and Fe^{3+} because of overlapping values for the quadrupole splittings (QS) of HS Fe^{2+} and LS Fe^{3+} as well as LS Fe^{2+} and HS Fe^{3+} (Li et al., 2006). Therefore, in order to understand the spin state of iron and its effects on the properties of Pv, it is important to distinguish between the effects of Fe^{2+} and Fe^{3+}. Andrault and Bolfan-Casanova (2001) demonstrated that Pv can be synthesized from 75 mol% $MgSiO_3$ + 25 mol% Fe_2O_3. We found that Pv with all Fe in Fe^{3+} can be synthesized as confirmed by our Mössbauer spectroscopy, although according to the literature, synthesizing Pv with all iron in Fe^{2+} is difficult (McCammon, 1997). We have performed SMS and XES on a sample with $Fe^{3+}/\Sigma Fe = 1$ in the laser-heated diamond anvil cell (DAC), allowing for reliable assignment of spin state. In order to study the effect of the spin transition on the equation of state of Pv, we performed XRD on ferric Pv and compared it to that of Mg-endmember Pv measured using a common pressure medium (Ar) and pressure standard (Au) (Lundin et al., 2008). This allows for comparison between the systems that would not otherwise be possible due to varied levels of deviatoric stress and disagreement among common pressure scales at high pressure (Shim et al., 2001a; Fei et al., 2004).

2. Experimental procedure

A glass starting material was synthesized from a mixture of $0.9MgSiO + 0.1Fe_2O_3$ (95% enriched ^{57}Fe) using the containerless laser levitation method in an O_2 atmosphere in order to prevent reduction during melting (Tangeman et al., 2001). The composition was examined using electron microprobe on a randomly selected glass bead. Measurements revealed a very homogeneous starting material. However, there was a 5% and 3% loss of Mg and Fe, respectively, during melting due to the volatility of these elements. The amount of oxygen and iron measured using electron microprobe indicates that all iron exists as Fe^{3+}, which is also consistent with our Mössbauer results.

The glasses were ground to a powder and mixed with 10 wt.% Au for use as an internal pressure standard (Tsuchiya, 2003) for the XRD study. For SMS, a couple of ruby grains were placed at the edge of the sample for pressure determination (Mao et al., 1986) at 47–63 GPa. Above this pressure the first-order Raman mode of diamond, the anvil material, was used to estimate pressure (Sun et al., 2005). Pressure in XES was determined by ruby.

Symmetric type DACs were used in all experiments. Diamonds with a culet size of 200 μm were used for measurements with a peak pressure less than 75 GPa. Above this pressure diamonds with 100 or 150 μm beveled culets were used. Measurements in each respective data set were taken from multiple sample loadings.

For XRD and SMS, the sample powder was pressed to a foil of ~10 μm thickness, and loaded into a preindented Re gasket. Ar was cryogenically loaded into the DAC, acting as both an insulating and a pressure medium. A few spacer grains of the starting material were used to keep the sample foil from having direct contact with the diamond anvils, because diamond has a high thermal conductivity. Ar diffraction lines are well resolved to the highest pressures of our study, confirming the presence of a significant amount of medium (Fig. 1). Both the hexagonal close-packed (hcp) and face-centered cubic structures of Ar are observed in some of our diffraction patterns, likely due to the inclusion of a small amount of nitrogen during cryogenic loading of Ar, which stabilizes the hcp phase (Wittlinger et al., 1997; Catalli et al., 2008). For XES, 3 mm diameter Be gaskets with an initial central thickness of 100 μm were used. A sample platelet was pre-pressed and sandwiched between 5 μm layers of dried NaCl and loaded into the gasket hole.

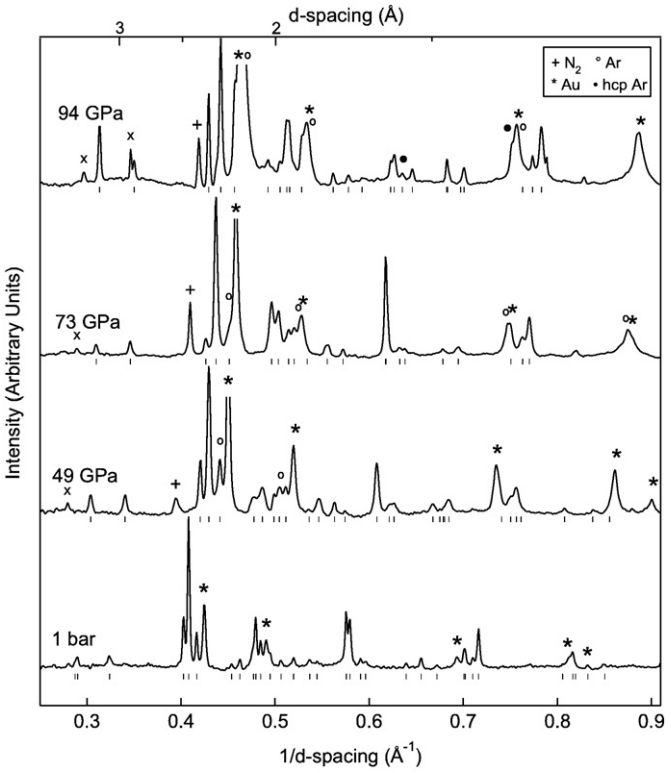

Fig. 1. High-pressure X-ray diffraction patterns of ferric Pv synthesized from glass starting material. Tick marks beneath each pattern show the locations of Pv peaks used in the unit-cell fitting (×: unknown lines, *: Au pressure standard, +: N_2, ○: Ar pressure medium, ●: h.c.p. Ar). Backgrounds were subtracted.

Angle dispersive XRD was performed at the GSECARS and HPCAT sectors of the Advanced Photon Source (APS). A monochromatic X-ray beam with energy of 30 or 28 keV was focused to a size smaller than $10 \times 20\ \mu m^2$. The diffraction images were collected using either a MarCCD detector or a Mar345 imaging plate. The downstream diamond anvil was mounted on an X-ray semi-transparent cBN backing plate, extending the measurable *d*-spacing to 1.1 Å. A total of 13–28 diffraction lines were used to constrain the volume of Pv using the UnitCell program (Holland and Redfern, 1997). The volume of Au was measured based on 2–5 diffraction lines and pressure was calculated using the scale of Tsuchiya (2003). The uncertainty in pressure given is the standard deviation in pressure based on the volume of gold calculated from each individual diffraction line.

SMS was performed at Sector 3 of APS. The X-ray beam was focused to an area of $6 \times 6\ \mu m^2$. The storage ring was operated in top-up mode with 24 bunches separated by 153 ns. Nuclear resonant scattering was measured in a time window of 15–130 ns following excitation. Data collection typically took 2 h (see Jackson et al., 2005; Sturhahn and Jackson, 2007 for more information). SMS data were fit using the CONUSS package (Sturhahn, 2000).

XES was performed at the HPCAT sector of APS. An 11.35 eV monochromatic X-ray beam was focused down to $30 \times 40\ \mu m^2$ on the sample. Emission was collected through the Be gasket. Collection time was typically 8–16 h. The sample and low-spin standard (Fe_2O_3) spectra have been aligned according to their centers of mass relative to a reference spectrum and normalized by total area following the method by Vankó et al. (2006). We used the spectrum of an iron foil, which has very low satellite peak intensity, for the reference spectrum in the analysis.

The Pv phase was synthesized by double-sided laser heating at 2000 K for 30 min at 50 GPa using an Nd:YLF laser at APS. In addition, at each pressure above 30 GPa, the sample was scanned with the laser at ~1800 K for 15 min to synthesize the stable structure at the new pressure and to anneal deviatoric stress. For SMS above 100 GPa, we did not anneal in order to avoid a phase transition from Pv to post-Pv (PPv) at high temperature (Murakami et al., 2004; Oganov and Ono, 2004; Shim et al., 2004). Laser annealing was not used on decompression in measurements conducted between 0 and 30 GPa, in order to prevent transformation to the lower-pressure phase.

3. Results

3.1. Effect of Fe^{3+} on the structure of Pv

In order to examine the stability of Pv with $Fe^{3+}/\Sigma Fe = 1$, we synthesized Pv at 45–50 GPa and 2000 K from a crystalline mixture of $0.1Fe_2O_3$ hematite + $0.9MgSiO_3$ enstatite and $0.9MgSiO_3 \cdot 0.1Fe_2O_3$ glass. After laser heating of the oxide mixture sample, the major diffraction lines are well explained by those of the *Pbnm* Pv structure, which is consistent with the earlier observation by Andrault and Bolfan-Casanova (2001). Furthermore, the diffraction patterns of Pv synthesized from the oxide mixture agree well with those of Pv synthesized from the glass starting material. These observations suggest the thermodynamic stability of ferric Pv over a $MgSiO_3 + Fe_2O_3$ mixture. However, we also observed weak diffraction lines from the high-pressure phases of SiO_2 and Fe_2O_3 (Olsen et al., 1991; Kingma et al., 1995; Ono et al., 2004; Shim et al., 2009) in some patterns of Pv synthesized from the oxide mixture. The existence of these minor lines may be due to inhomogeneity in the laser coupling or inhomogeneity in the sample mixture.

The synthesis of ferric Pv from glass was performed between 47 and 52 GPa and 2000 K. Pure *Pbnm* Pv was synthesized without evidence of other minor phases. Ferric Pv remains orthorhombic to at least 106 GPa. In several diffraction patterns there is an unknown line at ~3.4 Å that cannot be assigned to Pv, Au, Ar, Re or any known SiO_2 or Fe_2O_3 phases (Fig. 1). It shifts at a much greater rate with pressure than would be expected if it were diffraction from Pv, which suggests that it is unlikely related to Pv.

The glass starting material contained a slight excess of Si due to the volatile loss of Mg and Fe^{3+} during the containerless synthesis. Therefore, if the synthesized Pv has the same cation ratios as the glass starting material, it is possible that the synthesized Pv has some amount of oxygen vacancies through oxygen vacancy substitution, $Si_B^{4+} + \frac{1}{2}O^{2-} \rightarrow Fe_B^{3+} + \frac{1}{2}V_O^0$, where the subscripts denote crystallographic sites and V_O^0 denotes an oxygen vacancy (Navrotsky et al., 2003).

Alternatively, Fe^{3+} can enter Pv through charge coupled substitution, which will lead to an excess SiO_2 phase coexisting with the Pv phase for our starting material. Although no SiO_2 phases, stishovite or the $CaCl_2$-type, are evident in our diffraction patterns, this does not preclude the existence of an SiO_2 phase as the detection limit is likely ~5%. In addition, our SMS and XES suggest approximately equal weighting of Fe^{3+} (see Sections 2 and 3) into both the A and B sites of Pv, which does not support a significant amount of oxygen vacancies. Because computational studies suggested the stabilization of charge-coupled substitution over oxygen vacancy substitution for trivalent cations in Pv at higher pressure (Brodholt, 2000), we synthesized Pv only above 47 GPa, which should reduce the possibility of oxygen vacancies in ferric Pv.

We found that Fe^{3+} expands the volume of Pv relative to Mg-endmember more than Fe^{2+} between 0 and 106 GPa: 17 mol% Fe^{3+} expands the volume at 1 bar (V_0) by 2.1% whereas 15 mol% Fe^{2+} expands it by only 0.6% (Lundin et al., 2008) (Fig. 2). At 1 bar, HS Fe^{3+} is 45% larger than Si^{4+} whereas it is 11% smaller than Mg^{2+} (Shannon, 1976). Yet, HS Fe^{2+} is only 3% larger than Mg^{2+}. Therefore, our observation indicates that the expansion of the octahedra has a greater effect on the volume of Pv than the contraction of the dodecahedra.

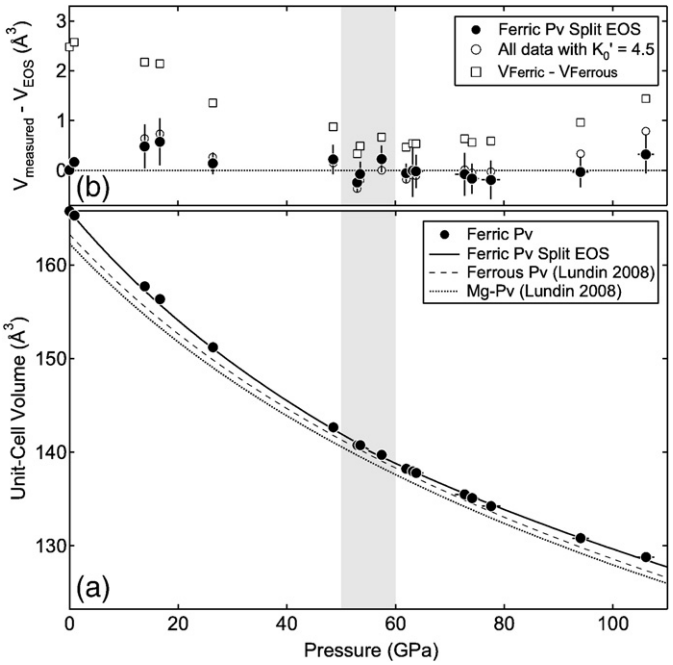

Fig. 2. (a) Measured volume of ferric Pv (black circles). The solid curve shows the EOS fit split at 55 GPa. Error bars are given as 1σ. Also shown for comparison are the EOSs of $MgSiO_3$ perovskite (dotted curve) and $(Mg_{0.85},Fe_{0.15})SiO_3$ (dashed curve) (Lundin et al., 2008). (b) Difference between the measured data and EOS fits. The solid and open circles are the residuals for the split EOS fit and the whole fit, respectively. The open squares are the volume difference between ferric and ferrous Pv. The error bar for ΔV estimated from both pressure and volume are shown for our best fit only. However, the same error bar can be applied also for the other fit residuals. The gray area is the pressure range where we found the completion of the Fe^{3+} spin transition.

Fe^{3+} also increases the axial ratios (c/a and b/a) relative to Mg-endmember Pv, whereas Fe^{2+} decreases them (Lundin et al., 2008) (Fig. 3). This suggests that Fe^{3+} increases the anisotropy of the unit cell of Pv whereas Fe^{2+} decreases it. Fe^{3+} enters into both the A and B

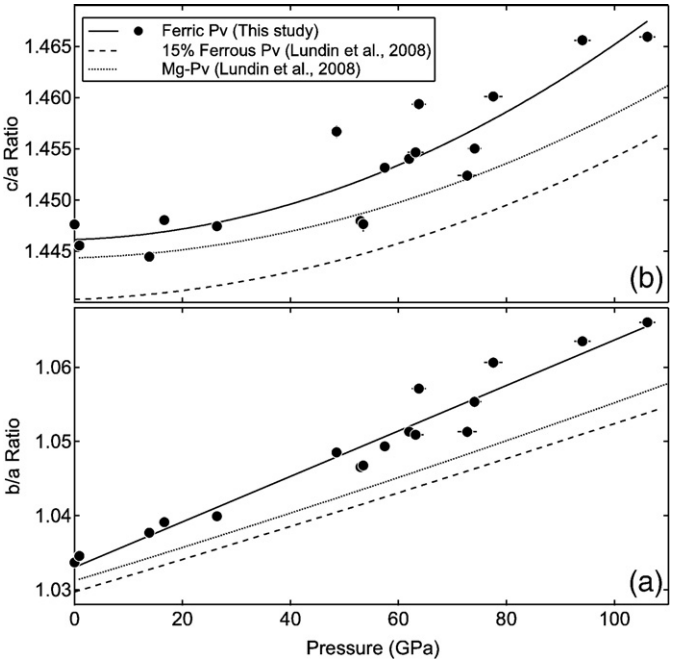

Fig. 3. Axial ratios, (a) b/a and (b) c/a, of Pv with different compositions. Ferric Pv is shown in solid circles, with the solid curves providing a guide for the eye. Ferrous Pv is shown by the dashed curves, and Mg-endmember Pv by the dotted curves (Lundin et al., 2008).

sites, according to our SMS, whereas Fe^{2+} enters only the A site. Therefore, Fe^{3+} will expand the volume of the octahedra, but it is smaller than Mg in the A site, and thus will induce more octahedral tilting, resulting in higher anisotropy of Pv.

3.2. Synchrotron Mössbauer spectroscopy

SMS was performed at a series of pressures between 47 and 136 GPa (Fig. 4). The spectra at 47 and 53 GPa consist of only two quantum beats while the spectra at 63 GPa and above consist of four quantum beats with a more regular spacing between 20 and 130 ns, indicating a change in the electronic configuration of Fe^{3+} between 53 and 63 GPa.

In order to extract Mössbauer parameters, the spectra were fit with a two Fe site model. Attempts were made for one and three site models, but the spectra require more than one site and three site models did not improve the fitting. The obtained Mössbauer parameters include the relative site weighting, quadrupole splitting (QS), the full-width at half maximum (FWHM) of the QS, and the relative center shift (ΔCS) between the two Fe sites.

The two Fe sites in ferric Pv show very different QS values, but with a small ΔCS (Fig. 5). The QS value can be affected by oxidation state, spin state (HS and LS), and coordination state (A and B sites). In this study, all iron in Pv is Fe^{3+}, making QS dependent primarily on spin state and coordination state. In general, LS Fe^{3+} has a larger QS (~2.0–3.5 mm/s) than HS Fe^{3+} (~0.0–1.5 mm/s). This has been shown to be the case in the rare-earth orthoferrite perovskites ($LaFeO_3$ and $PrFeO_3$) which have the same *Pbnm* perovskite structure: QS ≃ 2.4 mm/s was observed for LS Fe^{3+} in the B site (Xu et al., 2001; Rozenberg et al., 2005). Increased coordination number also increases QS but to a lesser degree (~0.5 mm/s) (Dyar et al., 2006). Therefore, the two Fe^{3+} sites we identify are distinguished more by their spin state rather than their coordination state and the low and high QS sites are assigned to HS and LS Fe^{3+}, respectively.

The visible change in the spectra between 53 and 63 GPa is related to an increase in the weighting of LS Fe^{3+} relative to HS, a slight drop in the QS of each site, a drastic reduction in the width of the QS of the HS site as well as a slight reduction in that of the LS site, and an increase in ΔCS (Fig. 5). No further changes occur in the SMS above 63 GPa up to 136 GPa (Figs. 4 and 5).

We interpret these observations as following. Below 50 GPa, HS Fe^{3+} exists in both the A and B sites and LS Fe^{3+} only exists in the B site. Because coordination also changes QS but to a lesser degree, the existence of HS Fe^{3+} in both sites results in the large QS distribution for the HS Fe^{3+} site. However, because LS Fe^{3+} exists only in the B site, it has a much smaller QS distribution (Fig. 5c).

At 50–60 GPa, all Fe^{3+} in the B site becomes LS and the A site is left with only HS Fe^{3+} (therefore, mixed spin), which makes the distributions of both sites small and similar to each other. This also explains an increase in the relative population of the LS Fe^{3+} site. The assignment of LS Fe^{3+} to the B site is also supported by computational predictions (Li et al., 2005; Stackhouse et al., 2007).

The relative population above 60 GPa remains nearly constant at 60:40, whereas 50:50 is expected if all HS Fe^{3+} are in the A site and all LS are in the B site. The relative population is obtained by assuming the same Mössbauer responses, such as recoil-free fractions, from each site, because no information exists. However, the two sites unlikely have the same Mössbauer responses (Hawthorne, 1988). A similar degree of offset in the site population was also found in the PPv phase of Fe_2O_3 (Shim et al., 2009) where Fe must exist in two different sites with equal weighting, as required by the crystal structure. This example demonstrates that a reasonable uncertainty for this parameter is ±10%. The fact that the QS distribution for the LS and HS sites becomes essentially the same above the transition suggests that they are in separate crystallographic sites, i.e., the A and B sites of Pv. In addition, as shown in Section 3.3, our XES indicates that the ratio between HS and LS Fe^{3+} above 50 GPa is 50:50 within experimental uncertainties. From these results, we conclude that Fe^{3+} substitutes into Pv through charge coupled substitution ($Mg_A^{2+} + Si_B^{4+} \rightarrow Fe_A^{3+} + Fe_B^{3+}$) rather than oxygen vacancy substitution.

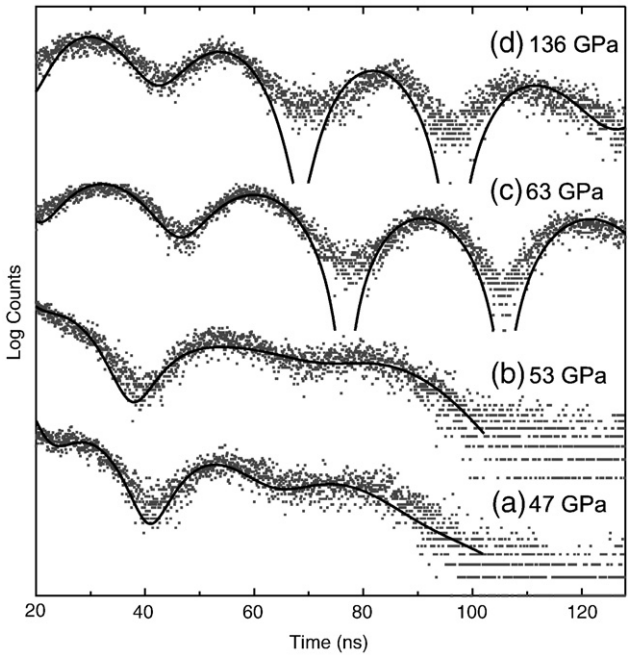

Fig. 4. Synchrotron Mössbauer spectra of ferric Pv at high pressure. The data points are shown as dots while the curves are the best fits using CONUSS. The relatively large gap between the fit and observed spectra at 60–80 and 100–120 ns is due to the logarithmic scale. The gap is only about 1–5% of the maximum intensity of the spectra which is comparable to misfits in other spectral regions.

3.3. X-ray emission spectroscopy

X-ray emission spectra of HS Fe consist of two main features: the main $K\beta_{1,3}$ peak near 7058 eV and the $K\beta'$ satellite at lower energy (Fig. 6). The $K\beta'$ intensity is proportional to the average spin number of iron in the sample, with a greater intensity equivalent to a higher spin sample (Badro et al., 1999). Also, Vankó et al. (2006) showed that the $K\beta_{1,3}$ peak position shifts to a lower energy with a reduction in the average spin of the sample.

We synthesized Pv at 50 GPa for XES. Between 48 and 67 GPa, no change in the $K\beta'$ intensity and the $K\beta_{1,3}$ peak position were found (Fig. 6). Upon decompression there is an increase in the $K\beta'$ intensity and the $K\beta_{1,3}$ peak position. These observations indicate that the HS to LS transition is a progressive transition with pressure up to 48 GPa, above which there is no change in average spin. Above 48 GPa, the $K\beta'$ intensity still remains higher than that in Fe_2O_3 with LS Fe^{3+} at 46 GPa (Badro et al., 2002), suggesting that some Fe^{3+} remains in HS in this pressure range.

Assuming that the spectrum measured at 0 GPa represents complete HS Fe^{3+}, we obtained the fraction of HS Fe^{3+} at high pressure (the inset in Fig. 6) using the difference in the satellite peak intensity from that of the LS Fe_2O_3 spectrum at 46 GPa by Badro et al. (2002). This reveals that the HS fraction decreases with pressure up to 48 GPa and then remains constant above that pressure at approximately 50%, within experimental uncertainties. The interpretation for the lower pressure range is possible from XES, as no data point exists below 40 GPa in SMS, while the interpretation for the high pressure range is in agreement with our SMS interpretation. We also note that quantitative analysis of XES is affected by the choice of reference spectrum. Unfortunately, appropriate standards for perovskite phases with all iron in HS Fe^{3+} and LS Fe^{3+} are not available. Considering that the structural difference would affect the XES less (Vankó et al., 2006),

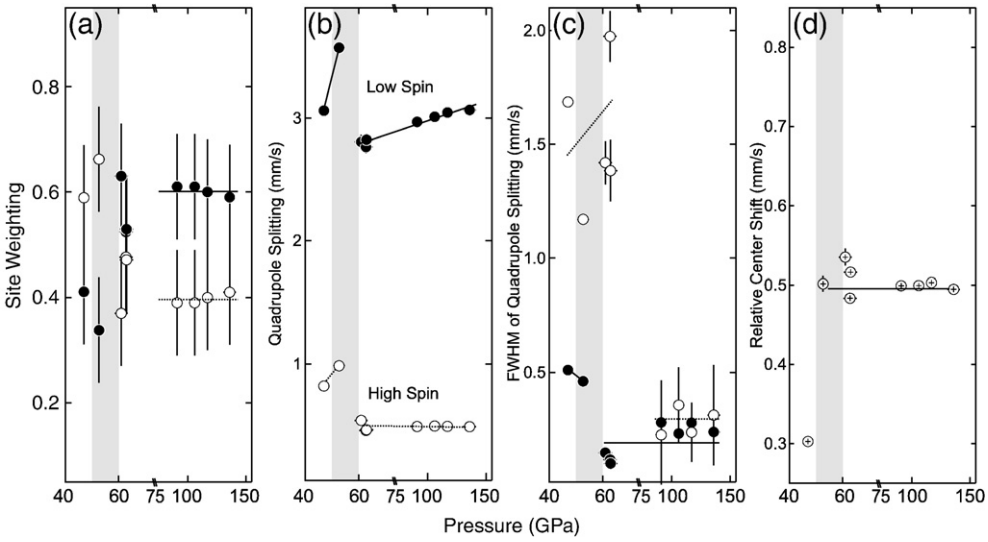

Fig. 5. Mössbauer parameters from fitting of data with CONUSS: (a) relative site weighting, (b) quadrupole splitting (QS), (c) full width at half maximum or distribution of QS values, and (d) relative center shift (ΔCS). Lines are guides for the eye. All parameters for the LS site are given as solid circles while parameters for the HS site are given as open circles. Note that the *x*-axis is split at 75 GPa and scaled differently above and below that pressure. The gray area is the pressure range where we found the completion of the Fe^{3+} spin transition in the B site.

a reasonable estimate for the uncertainty would be 10% for the spin number calculated from the satellite intensity.

While SMS suggests that the spin transition in the B site completes between 53 and 63 GPa, XES indicates 48 GPa. Considering experimental uncertainties, including different pressure media and different stress conditions along the radial (XES) and axial (SMS) directions of the DAC, we believe that the transition pressure likely exists between 48 and 63 GPa.

3.4. Equation of state

In order to constrain the equation of state (EOS), we measured the volume of ferric Pv synthesized from the glass starting material up to 106 GPa (Fig. 1). Because our data collected after heating above

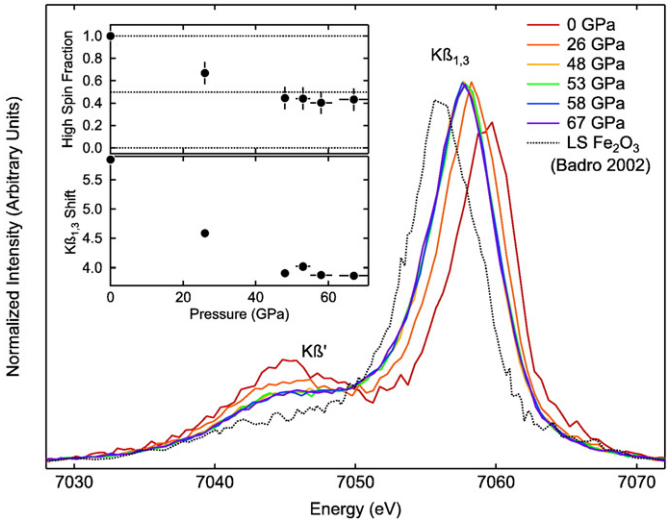

Fig. 6. X-ray emission spectra of ferric Pv at high pressure. The dotted curve is the spectrum of LS Fe_2O_3 at 46 GPa by (Badro et al., 2002). The top inset shows the HS fraction obtained from the Kβ' intensity difference (see the text for method). The Kβ' intensity difference is relative to LS Fe_2O_3 (Badro et al., 2002). A value of zero on the *y*-axis refers to all Fe^{3+} in LS (average spin = 1/2) and a value of 1.0 refers to all Fe^{3+} in HS (average spin = 5/2). The bottom inset shows in the position of the main K$\beta_{1,3}$ peak relative to the center of mass of the spectrum.

106 GPa appears to be within the Pv + PPv mixed phase region (Murakami et al., 2004; Mao et al., 2004; Shieh et al., 2006; Shim et al., 2008), we restrict our data presented to those inside the Pv stability field. Note that all the data points used for EOS fits are obtained after laser annealing to 2000 K except for the data points below 25 GPa. In order to prevent synthesis of a low-pressure phase, we did not laser anneal the samples below 25 GPa.

Fitting all of the *P*–*V* data between 0 and 106 GPa to the third-order Birch–Murnaghan (BM) equation gives a bulk modulus of $K_0 = 228 \pm 5$ GPa at 1 bar, with a pressure derivative of $K_0' = 4.5 \pm 0.3$ for V_0 fixed to 165.78 ± 0.03 Å^3, which was measured in this study. The K_0 and K_0' of ferric Pv are significantly lower and higher, respectively, than those of Mg-endmember and ferrous Pv measured by Lundin et al., (2008) using the same Au scale. This comparison indicates that Fe^{3+} makes Pv more compressible at lower pressure but less compressible at higher pressure.

We explore the compressibility of ferric Pv relative to ferrous Pv by calculating the differences between the measured volume of ferric (17 mol%) Pv and the EOS of ferrous (15 mol%) Pv (Lundin et al., 2008), *V* (ferricPv) − *V* (ferrousPv) (open squares in Fig. 2b). The volume difference decreases with pressure below 55 GPa, suggesting that the compressibility of ferric Pv is higher than ferrous Pv. Above 50–60 GPa, the volume difference increases with pressure, indicating that ferric Pv becomes less compressible. In other words, the compressibility changes near the pressure range where our SMS and XES results indicate the completion of the HS → LS transition in the B site. However, some systematic trends still remain in the fit residual (open circles in Fig. 2b).

In order to examine the statistical significance of the systematic trend observed in *V* (ferricPv) − *V* (ferrousPv) and the fit residual, we consider all the possible uncertainty sources. The largest source is from the uncertainty in the absolute pressure scale, which should be ~5%. Following the method by Jackson and Rigden (1996), we propagated the uncertainty in pressure using $\sigma(\Delta V)^2 = \sigma(V)^2 + \sigma(P)^2(V/K)^2$ and presented them in Fig. 2b. Without propagating the uncertainty in this way, the error bar would only reflect the precision of the volume measurements and not take into account the pressure uncertainty. Even after considering this uncertainty, the trend in *V* (ferricPv) − *V* (ferrousPv) remains significant (the open squares in Fig. 2b).

Because the spin transition is completed and the trend in *V* (ferricPv) − *V* (ferrousPv) changes near 50–60 GPa, we fit our *P*–*V*

data with two different pressure ranges, above and below 55 GPa. Because of the strong correlation between K_0 and K'_0 (Bell et al., 1987), the second-order BM equation is used for both pressure ranges. The method described in Sata et al. (2002) and Shim et al. (2008) was used by setting the reference state at 55 GPa instead of 1 bar, because V_0 for the trend above 55 GPa is unknown. This attempt somewhat improves the fitting over using the entire pressure range in one EOS, even though K'_0 is fixed to 4. We obtained $K_{55\ \mathrm{GPa}} = 439 \pm 2$ GPa for the lower-pressure data and $K_{55\ \mathrm{GPa}} = 501 \pm 17$ GPa for the higher-pressure data, which is a $14 \pm 4\%$ increase in bulk modulus at the spin transition. However, density does not change at 55 GPa (Fig. 7a,b). The fit residual of this scheme is less systematic and close to zero considering the uncertainty.

When the latter fitting results are projected to 1 bar, we obtained $K_0 = 237 \pm 3$ GPa for the lower-pressure data and $K_0 = 304 \pm 20$ GPa for the higher-pressure data. Compared with the bulk moduli of 15 mol% ferrous and Mg-endmember Pv, 259–261 GPa (Lundin et al., 2008), which used the same pressure scale and the same pressure medium, this fitting result suggests that Fe^{3+} makes Pv more compressible during the spin transition, but less compressible after the completion of the spin transition. This was also observed in fitting all the data points in one third-order BM equation, suggesting that the trend is robust and does not depend on the fitting schemes.

Below 50–60 GPa, compression in ferric Pv is accommodated by both lattice compression and the gradual spin collapse of Fe^{3+} in the B site. For comparison, across the spin transition in ferropericlase, the size of Fe^{2+} appears to decrease by 10% (Fei et al., 2007). Therefore, these compressional mechanisms at low pressure would result in a greater compressibility of the structure during the gradual spin transition. After the completion of the gradual Fe^{3+} spin transition in the B site, volume reduction is only achieved by lattice compression, which is reflected by the increase in bulk modulus after the spin transition.

4. Implications for the spin state of iron in Pv

Our results provide useful information for the spin state of iron in Pv, which has recently been the subject of much debate (Badro et al., 2004; Li et al., 2004; Jackson et al., 2005; Lin et al., 2008; McCammon et al., 2008). A two step decrease in the satellite peak intensity in the XES of Al-free Pv found by Badro et al. (2004) was not well understood, because of the coexistence of Fe^{2+} and Fe^{3+}. Interestingly, the pressure range where the first drop was observed (40–60 GPa) coincides with the pressure range where we observed a gradual spin transition of Fe^{3+} in the B site. Therefore, the drop in the HS population at lower pressure may be related to the spin transition of Fe^{3+}.

In contrast, Li et al. (2004) reported a gradual loss of spin in both Al-bearing and Al-free Pv in their XES. The gradual loss in Al-bearing Pv may be due to the effects of Al. The smaller pressure range and fewer data points for Al-free Pv in Li et al. (2004) make comparison difficult. Also, Badro et al. (2004) annealed Pv, whereas Li et al. (2004) did not, which could result in the difference.

Jackson et al. (2005) reported a gradual decrease in ΔCS below 70 GPa where CS becomes insensitive to pressure in their SMS of Pv. They interpreted that the change might be related to a spin transition in Fe^{3+}. In fact, our results confirm this interpretation. We note that our measurements make unambiguous interpretation possible as Pv contains only Fe^{3+} in our study.

In computational studies, Stackhouse et al. (2007) and Zhang and Oganov (2006) found that Fe^{3+} in the B site is LS spin at all lower mantle pressures, and undergoes a HS to LS transition in the A site at 60–150 GPa. Our results on the spin state of Fe^{3+} in the B site are largely consistent, as our XES results show that LS Fe^{3+} exists in Pv at 26 GPa (Fig. 6). The difference here, is that not all Fe^{3+} in the B site is LS until higher pressures. We do not see a spin transition in the A site of Pv up to 136 GPa, which does not rule out the possibility at higher pressures.

5. Implications for the lower mantle

Because the Fe^{3+} spin transition occurs only in the B site, it is important to know whether mantle silicate Pv contains Fe^{3+} in the B site. A single crystal study at 1 bar suggested that Fe^{3+} may exist only in the A site, whereas Al preferentially enters the B site through charge coupled substitution (Vanpeteghem et al., 2006). This is perhaps

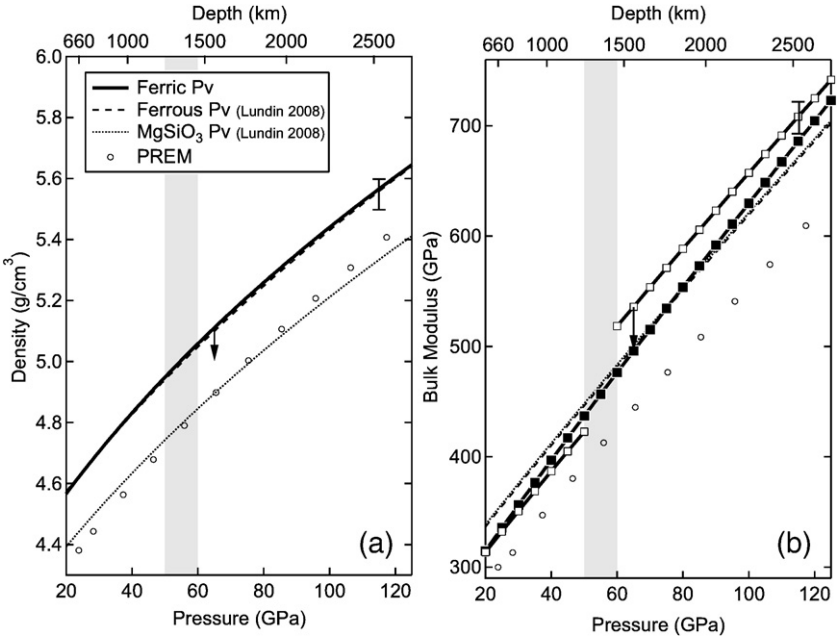

Fig. 7. Profiles of (a) density and (b) bulk modulus for ferric Pv (thick solid lines), ferrous Pv (thin dashed curves), and Mg-endmember Pv (thin dotted curves) (Lundin et al., 2008), and PREM (Dziewonski and Anderson, 1981) (open circles). In (b), we present bulk modulus profiles calculated from fitting all the data in one third-order BM equation (thick solid line with solid squares) and fitting the data to two second-order BM equations by dividing them at 55 GPa (thick solid line with open squares). Note that the profiles for Pv are calculated at 300 K. The arrows shown represent the expected thermal effect at 2000 K on these parameters for Mg-endmember Pv (Fiquet et al., 2000). The gray area is the pressure range where we found the completion of the Fe^{3+} spin transition.

because HS Fe^{3+} is 15–20% larger than Al when octahedrally coordinated (Shannon, 1976). However, after the spin transition at high pressure, LS Fe^{3+} is essentially the same size as Al, only about 2% larger (Shannon, 1976). Therefore, they are likely to compete for the B site at high pressure. Our preliminary SMS results for Pv with equal amounts of Fe^{3+} and Al show that 30–50% of Fe^{3+} exists in the B site at pressures above 40 GPa, supporting this argument (Catalli et al., in preparation).

In Fig. 7, we compare the density and bulk modulus of ferric Pv with those of ferrous Pv and the Earth's lower mantle, taken from the Preliminary Reference Earth Model (PREM) (Dziewonski and Anderson, 1981). Because our measurements are conducted at 300 K, we present profiles at 300 K. For better comparison with PREM, the black arrow in each figure shows the approximate thermal effect (2000 K) (Fig. 7) which was calculated based on the thermal parameters for Mg-endmember Pv (Fiquet et al., 2000; Shim and Duffy, 2000). As found in our study, the completion of the Fe^{3+} spin transition at 50–60 GPa does not result in a noticeable effect on density, but does cause changes in bulk modulus.

An important question for geophysical application is whether the bulk modulus increase, or bulk sound speed increase, would be sharp at lower-mantle temperatures. Because of the insufficient data coverage in our SMS and XES and limited resolution in the *P–V* dataset, it is unclear whether there would be a sharp or broad boundary between the pressure regime where the gradual spin pairing occurs (low pressure regime) and the pressure regime after the completion of the spin transition (high pressure regime). Therefore, we consider both the sharp (fitting the data to two second-order BM equations split at 55 GPa) and broad (fitting the all data points to one third-order BM equation) cases in Fig. 7b. Even if it is sharp, it is possible that temperature or composition would broaden it (Sturhahn et al., 2005; Li et al., 2005; Lin et al., 2007; Stackhouse et al., 2007). Also, these two factors can influence the pressure (or depth) where the boundary between the two regimes exists (Sturhahn et al., 2005; Hofmeister, 2006; Bengtson et al., 2008).

If the transition is sharp in the mantle (the solid line with open squares in Fig. 7), it would result in a velocity discontinuity (but without a density change) in the mid lower mantle, providing a useful probe for the existence of Fe^{3+} in the lower mantle. If the transition is gradual in the Earth's mantle (the solid line with solid squares in Fig. 7), it will affect the velocity profile at the mid to lowermost mantle, which, combined with laboratory measured density/velocity profiles, is critical for constraining the composition of the lower mantle (Stixrude et al., 1992). The sharpness of the boundary between the two pressure regimes found in this study remains to be investigated in future studies. Nevertheless, our study shows that the spin state of Fe^{3+} changes at mid lower mantle pressures and the change is localized to a specific crystallographic site (B) in Pv. Also, this transition likely affects seismic velocities in the lower mantle.

6. Conclusions

X-ray emission spectroscopy on Fe^{3+}-bearing $MgSiO_3$ perovskite reveals a gradual spin transition from high-spin to mixed-spin completing near 50 GPa. Synchrotron Mössbauer spectroscopy results demonstrate that Fe^{3+} in the B site of perovskite undergoes a spin transition to 50–60 GPa where all Fe^{3+} in the B site becomes low spin. However, Fe^{3+} in the A site remains high-spin throughout lower-mantle pressures. Our volume measurements at high pressure indicate that there is no discontinuous change in the density of ferric perovskite associated with the completion of the spin transition. However, equation of state fitting indicates that the bulk modulus increases at the completion of the spin transition. In addition, we found that the charge coupled substitution of Fe^{3+}–Fe^{3+} for Mg–Si increases the orthorhombic distortion of the perovskite structure, in contrast to substituting predominantly Fe^{2+} for the A site, which reduces the distortion. The elasticity change found at the completion of the Fe^{3+} spin transition can be a useful probe for seismic investigations of the valence state of iron and compositional heterogeneities in the lower mantle.

Acknowledgments

We thank N. Chatterjee, J. Hustoft, B. Grocholski, S. Slotznick, and D. LaBounty for experimental assistance and two anonymous reviewers for their comments on the manuscript. Measurements performed at GeoSoilEnviroCARS, APS, were supported by the National Science Foundation (NSF), Department of Energy (DOE) and the State of Illinois. Portions of this work performed at HPCAT, APS, were supported by DOE, NSF, and the W. M. Keck Foundation. Use of Sector 3 was partially supported by COMPRES, the Consortium for Materials Properties Research in Earth Sciences. Use of the APS was supported by the DOE. K.C. is supported by the DOE NNSA Stewardship Science Graduate Fellowship. This work is supported by NSF to S.H.S. (EAR0738655).

References

Andrault, D., Bolfan-Casanova, N., 2001. High-pressure phase transformations in the $MgFe_2O_4$ and Fe_2O_3–$MgSiO_3$ systems. Phys. Chem. Miner. 28 (3), 211–217.
Andrault, D., Bolfan-Casanova, N., Guignot, N., 2001. Equation of state of lower mantle (Al, Fe)–$MgSiO_3$ perovskite. Earth Planet. Sci. Lett. 193 (3–4), 501–508.
Auzende, A.-L., Badro, J., Ryerson, F.J., Weber, P.K., Fallon, S.J., Addad, A., Siebert, J., Fiquet, G., 2008. Element partitioning between magnesium silicate perovskite and ferropericlase: new insights into bulk lower-mantle geochemistry. Earth Planet. Sci. Lett. 269 (1–2), 164–174.
Badro, J., Struzhkin, V.V., Shu, J.F., Hemley, R.J., Mao, H.-K., 1999. Magnetism in FeO at megabar pressures from X-ray emission spectroscopy. Phys. Rev. Lett. 83 (20), 4101–4104.
Badro, J., Fiquet, G., Struzhkin, V.V., Somayazulu, M., Mao, H.-K., Shen, G., Le Bihan, T., 2002. Nature of the high-pressure transition in Fe_2O_3 hematite. Phys. Rev. Lett. 89 (20), 205504.
Badro, J., Rueff, J.-P., Vankó, G., Monaco, G., Fiquet, G., Guyot, F., 2004. Electronic transitions in perovskite: possible nonconvecting layers in the lower mantle. Science 305, 383–386.
Bell, P.M., Mao, H.-K., Xu, J.A., 1987. Error analysis of parameter-fitting in equations of state for mantle minerals. In: Manghnani, M.H., Syono, Y. (Eds.), High pressure research in mineral physics. Terra Scientific Publishing Company, pp. 447–454.
Bengtson, A., Persson, K., Morgan, D., 2008. Ab initio study of the composition dependence of the pressure-induced spin crossover in perovskite $(Mg_{1-x}Fe_x)SiO_3$. Earth Planet. Sci. Lett. 265, 535–545.
Bengtson, A., Li, J., Morgan, D., 2009. Mössbauer modeling to interpret the spin state of iron in (Mg, Fe)SiO_3 perovskite. Geophys. Res. Lett. 36, L15301.
Brodholt, J.P., 2000. Pressure-induced changes in the compression mechanism of aluminous perovskite in the Earth's mantle. Nature 407, 620–622.
Catalli, K., Shim, S.-H., Prakapenka, V.B., 2008. A crystalline-to-crystalline transition in $Ca(OH)_2$ at 8 GPa and room temperature. Geophys. Res. Lett. 35, L05312.
Cohen, R.E., Mazin, I.I., Isaak, D.G., 1997. Magnetic collapse in transition metal oxides at high pressure: implications for the Earth. Science 275, 654–657.
Dyar, M.D., Agresti, D.G., Schaefer, M.W., Grant, C.A., Sklute, E.C., 2006. Mössbauer spectroscopy of Earth and planetary materials. Annu. Rev. Earth Planet. Sci. 34, 83–125.
Dziewonski, A.M., Anderson, D.L., 1981. Preliminary reference Earth model. Phys. Earth Planet. Inter. 25 (4), 297–356.
Fei, Y., Li, J., Hirose, K., Minarik, W., Van Orman, J., Sanloup, C., van Westrenen, W., Komabayashi, T., Funakoshi, K., 2004. A critical evaluation of pressure scales at high temperatures by in situ X-ray diffraction measurements. Phys. Earth Planet. Inter. 143–144, 515–526.
Fei, Y., Zhang, L., Corgne, A., Watson, H., Ricolleau, A., Meng, Y., Prakapenka, V.B., 2007. Spin transition and equation of state of (Mg, Fe)O solid solution. Geophys. Res. Lett. 34, L17307.
Fiquet, G., Dewaele, A., Andrault, D., Kunz, M., Le Bihan, T., 2000. Thermoelastic properties and crystal structure of $MgSiO_3$ perovskite at lower mantle pressure and temperature conditions. Geophys. Res. Lett. 27 (1), 21–24.
Frost, D.J., Liebske, C., Langenhorst, F., McCammon, C.A., Trønnes, R.G., Rubie, D.C., 2004. Experimental evidence for the existence of iron-rich metal in the Earth's lower mantle. Nature 428 (6981), 409–412.
Goncharov, A.F., Haugen, B.D., Struzhkin, V.V., Beck, P., Jacobsen, S.D., 2008. Radiative conductivity in the Earth's lower mantle. Nature 456 (13), 231–234.
Hawthorne, F.C. (Ed.), 1988. Spectroscopic methods in mineralogy and geology: Reviews in Mineralogy, vol. 18. Mineralogical Society of America.
Hofmeister, A.M., 2006. Is low-spin Fe^{2+} present in Earth's mantle? Earth Planet. Sci. Lett. 243 (1–2), 44–52.
Holland, T.J.B., Redfern, S.A.T., 1997. Unit cell refinement from powder diffraction data: the use of regression diagnostics. Mineral. Mag. 61, 65–77.

Jackson, I., Rigden, S.M., 1996. Analysis of P–V–T data: constraints on the thermoelastic properties of high-pressure minerals. Phys. Earth Planet. Inter. 96 (2–3), 85–112.
Jackson, J.M., Sturhahn, W., Shen, G.Y., Zhao, J.Y., Hu, M.Y., Errandonea, D., Bass, J.D., Fei, Y.W., 2005. A synchrotron Mössbauer spectroscopy study of (Mg, Fe)SiO_3 perovskite up to 120 GPa. Am. Mineral. 90 (1), 199–205.
Keppler, H., Dubrovinsky, L.S., Narygina, O., Kantor, I., 2008. Optical absorption and radiative conductivity of silicate perovskite to 125 gigapascals. Science 322, 1529–1532.
Kesson, S.E., Fitz Gerald, J.D., Shelley, J.M., 1998. Mineralogy and dynamics of a pyrolite lower mantle. Nature 393, 252–255.
Kingma, K.J., Cohen, R.E., Hemley, R.J., Mao, H.-K., 1995. Transformation of stishovite to a denser phase at lower-mantle pressures. Nature 374, 243–245.
Knittle, E., Jeanloz, R., 1987. Synthesis and equation of state of (Mg, Fe)SiO_3 perovskite to over 100 gigapascals. Science 235 (4789), 668–670.
Lee, K.K.M., O'Neill, B., Panero, W.R., Shim, S.H., Benedetti, L.R., Jeanloz, R., 2004. Equations of state of the high-pressure phases of a natural peridotite and implications for the Earth's lower mantle. Earth Planet. Sci. Lett. 223 (3–4), 381–393.
Li, J., Struzhkin, V.V., Mao, H.-K., Shu, J., Hemley, R.J., Fei, Y., Mysen, B., Dera, P., Prakapenka, V.B., Shen, G., 2004. Electronic spin state of iron in lower mantle perovskite. Proc. Natl. Acad. Sci. U. S. A. 101 (39), 14027–14030.
Li, L., Brodholt, J.P., Stackhouse, S., Weidner, D.J., Alfredsson, M., Price, G.D., 2005. Electronic spin state of ferric iron in Al-bearing perovskite in the lower mantle. Geophys. Res. Lett. 32, L17307.
Li, J., Sturhahn, W., Jackson, J.M., Struzhkin, V.V., Lin, J.F., Zhao, J., Mao, H.K., Shen, G., 2006. Pressure effect on the electronic structure of iron in (Mg, Fe)(Si, Al)O_3 perovskite: a combined synchrotron Mössbauer and X-ray emission spectroscopy study up to 100 GPa. Phys. Chem. Miner. 33, 575–585.
Lin, J.-F., Vankó, G., Jacobsen, S.D., Iota, V., Struzhkin, V.V., Prakapenka, V.B., Kuznetsov, A., Yoo, C.-S., 2007. Spin transition zone in Earth's lower mantle. Science 317, 1740–1743.
Lin, J.-F., Watson, H., Vankó, G., Alp, E.E., Prakapenka, V.B., Dera, P., Struzhkin, V.V., Kubo, A., Zhao, J., McCammon, C., Evans, W.J., 2008. Intermediate-spin ferrous iron in lowermost mantle post-perovskite and perovskite. Nat. Geosci. 1, 688–691.
Liu, L.-G., 1976. The high-pressure phases of $MgSiO_3$. Earth Planet. Sci. Lett. 31, 200–208.
Lundin, S., Catalli, K., Santillán, J., Shim, S.-H., Prakapenka, V.B., Kunz, M., Meng, Y., 2008. Effect of Fe on the equation of state of mantle silicate perovskite over 1 Mbar. Phys. Earth Planet. Inter. 168, 97–102.
Mao, H.-K., Xu, J., Bell, P.M., 1986. Calibration of the ruby pressure gauge to 800 kbar under quasihydrostatic conditions. J. Geophys. Res. 91, 4673–4676.
Mao, W.L., Shen, G.Y., Prakapenka, V.B., Meng, Y., Campbell, A.J., Heinz, D.L., Shu, J.F., Hemley, R.J., Mao, H.K., 2004. Ferromagnesian postperovskite silicates in the D″ layer of the Earth. Proc. Natl. Acad. Sci. U. S. A. 101 (45), 15867–15869.
McCammon, C., 1997. Perovskite as a possible sink for ferric iron in the lower mantle. Nature 387, 694–696.
McCammon, C., 2005. The paradox of mantle redox. Science 308, 807–808.
McCammon, C., Kantor, I., Narygina, O., Rouquette, J., Ponkratz, U., Sergueev, I., Mezouar, M., Prakapenka, V.B., Dubrovinsky, L., 2008. Stable intermediate-spin ferrous iron in lower-mantle perovskite. Nat. Geosci. 1 (10), 684–687.
Murakami, M., Hirose, K., Kawamura, K., Sata, N., Ohishi, Y., 2004. Post-perovskite phase transition in $MgSiO_3$. Science 304 (5672), 855–858.
Navrotsky, A., Schoenitz, M., Kojitani, H., Xu, H.W., Zhang, J.Z., Weidner, D.J., Jeanloz, R., 2003. Aluminum in magnesium silicate perovskite: formation, structure, and energetics of magnesium-rich defect solid solutions. J. Geophys. Res. 108 (B7), 2330.
Oganov, A.R., Ono, S., 2004. Theoretical and experimental evidence for a post-perovskite phase of $MgSiO_3$ in Earth's D″ layer. Nature 430, 445–448.
Olsen, J.S., Cousins, S.S.G., Gerward, L., Jhans, H., Sheldon, B.J., 1991. A study of the crystal structure of Fe_2O_3 in the pressure range up to 65 GPa using synchrotron radiation. Phys. Scr. 43, 327–330.
Ono, S., Kikegawa, T., Ohishi, Y., 2004. High-pressure phase transition of hematite, Fe_2O_3. J. Phys. Chem. Solids 65, 1527–1530.
Rozenberg, G., Pasternak, M., Xu, W., Dubrovinsky, L., Carlson, S., Taylor, R., 2005. Consequences of pressure-instigated spin crossover in *R*FeO_3 perovskites; a volume collapse with no symmetry modification. Europhys. Lett. 71, 228–234.
Sata, N., Shen, G., Rivers, M.L., Sutton, S.R., 2002. Pressure–volume equation of state of the high-pressure *B2* phase of NaCl. Phys. Rev. B 65, 104114.
Shannon, R.D., 1976. Revised effective ionic radii and systematic studies of interatomic distances in halides and chalcogenides. Acta Crystallogr. A A32, 751–767.
Shieh, S.R., Duffy, T.S., Kubo, A., Shen, G.Y., Prakapenka, V.B., Sata, N., Hirose, K., Ohishi, Y., 2006. Equation of state of the postperovskite phase synthesized from a natural (Mg, Fe)SiO_3 orthopyroxene. Proc. Natl. Acad. Sci. U. S. A. 103 (9), 3039–3043.
Shim, S.-H., Duffy, T.S., 2000. Constraints on the P–V–T equation of state of $MgSiO_3$ perovskite. Am. Mineral. 85 (2), 354–363.
Shim, S.-H., Duffy, T.S., Shen, G.Y., 2001a. The post-spinel transformation in Mg_2SiO_4 and its relation to the 660-km seismic discontinuity. Nature 411 (6837), 571–574.
Shim, S.-H., Duffy, T.S., Shen, G.Y., 2001b. Stability and structure of $MgSiO_3$ perovskite to 2300-kilometer depth in Earth's mantle. Science 293 (5539), 2437–2440.
Shim, S.-H., Duffy, T.S., Jeanloz, R., Shen, G., 2004. Stability and crystal structure of $MgSiO_3$ perovskite to the core–mantle boundary. Geophys. Res. Lett. 31 (10), L10603.
Shim, S.-H., Catalli, K., Hustoft, J., Kubo, A., Prakapenka, V.B., Kunz, M., 2008. Crystal structure and thermoelastic properties of (Mg0.91, Fe0.09)SiO_3 postperovskite up to 135 GPa and 2700 K. Proc. Natl. Acad. Sci. U. S. A. 105 (21), 7382–7386.
Shim, S.-H., Bengtson, A., Morgan, D., Sturhahn, W., Catalli, K., Zhao, J., Lerche, M., Prakapenka, V.B., 2009. Electronic and magnetic structures of the postperovskite-type Fe_2O_3 — implications for planetary magnetic records and deep interior transitions. Proc. Natl. Acad. Sci. U. S. A. 106, 5508–5512.
Stackhouse, S., Brodholt, J.P., Price, G.D., 2007. Electronic spin transitions in iron-bearing $MgSiO_3$ perovskite. Earth Planet. Sci. Lett. 253 (1–2), 282–290.
Stixrude, L., Hemley, R.J., Fei, Y., Mao, H.-K., 1992. Thermoelasticity of silicate perovskite and magnesiowüstite and stratification of Earth's mantle. Science 257, 1099–1101.
Sturhahn, W., 2000. CONUSS and PHOENIX: evaluation of nuclear resonant scattering data. Hyperfine Interact. 125 (1–4), 149–172.
Sturhahn, W., Jackson, J.M., 2007. Geophysical applications of nuclear resonant spectroscopy. In: Ohtani, E. (Ed.), Advances in High-Pressure Mineralogy. The Geological Society of America, pp. 157–174.
Sturhahn, W., Jackson, J.M., Lin, J.F., 2005. The spin state of iron in minerals of Earth's lower mantle. Geophys. Res. Lett. 32 (12), L12307.
Sun, L., Ruoff, A., Stupian, G., 2005. Convenient optical pressure gauge for multimegabar pressures calibrated to 300 GPa. Appl. Phys. Lett. 86, 014103.
Tangeman, J.A., Phillips, B.L., Navrotsky, A., Weber, J.K.R., Hixson, A.D., Key, T.S., 2001. Vitreous forsterite (Mg_2SiO_4): synthesis, structure, and thermochemistry. Geophys. Res. Lett. 28 (13), 2517–2520.
Tsuchiya, T., 2003. First-principles prediction of the P–V–T equation of state of gold and the 660-km discontinuity in Earth's mantle. J. Geophys. Res. 108 (B10), 2462.
Umemoto, K., Wentzcovitch, R.M., Yu, Y.G., Requist, R., 2008. Spin transition in (Mg, Fe)SiO_3 perovskite under pressure. Earth Planet. Sci. Lett. 276, 198–206.
Vankó, G., Neisius, T., Molnár, G., Renz, F., Kárpáti, S., Shukla, A., de Groot, M.F., 2006. Probing the 3d spin momentum with X-ray emission spectroscopy: the case of molecular-spin transitions. J. Phys. Chem. B 110, 11647–11653.
Vanpeteghem, C.B., Zhao, J., Angel, R.J., Ross, N.L., Bolfan-Casanova, N., 2006. Crystal structure and equation of state of $MgSiO_3$ perovskite. Geophys. Res. Lett. 33, L03306.
Wittlinger, J., Fischer, R., Werner, S., Schneider, J., Schulz, H., 1997. High-pressure study of hcp-argon. Acta Crystallogr. B 53 (5), 745–749.
Xu, Y., McCammon, C., Poe, B.T., 1998. The effect of alumina on the electrical conductivity of silicate perovskite. Science 282, 922–924.
Xu, W.M., Naaman, O., Rozenberg, G., Pasternak, M.P., Taylor, R.D., 2001. Pressure-induced breakdown of a correlated system: the progressive collapse of the Mott–Hubbard state of *R*FeO_3. Phys. Rev. B 64, 094411.
Zhang, F.W., Oganov, A.R., 2006. Valence state and spin transitions of iron in Earth's mantle silicates. Earth Planet. Sci. Lett. 249 (3–4), 436–443.

nation of the galactic plasma wind.

Bertram Schwarzschild

References

1. J. P. Wefel et al. (ATIC collaboration), in *Proceedings of the 30th International Cosmic Ray Conference.*, R. Caballero et al., eds., Universidad Nacional Autonomica, Mexico City (2008), vol. 2, p. 31; H. S. Ahn et al. (CREAM collaboration), *Astrophys. J. Lett.* **714**, L89 (2010).
2. O. Adriani et al. (PAMELA collaboration), *Science* **332**, 69 (2011).
3. V. I. Zatsepin, N. V. Sokolskaya, *Astron. Astrophys.* **458**, 1 (2006).
4. Y. Butt, *Nature* **460**, 701 (2009).
5. The graphic compilation, by P. Boyle and D. Müller, appears in K. Nakumura et al. (Particle Data Group), *J. Phys. G* **37**, 075021 (2010).

Calculations clarify the role of minerals' electron spins in Earth's mantle

Laboratory measurements of the spin states are indirect and prone to ambiguities.

When a transition-metal compound is subject to high pressure, its electronic spin state can change, which in turn can change its material properties. That spin-state crossover is of geophysical relevance because of the iron-bearing minerals in Earth's mantle and because material properties affect the speed of seismic waves. But the most abundant mantle mineral—Fe-bearing magnesium silicate perovskite (Pv)—is a challenge to study, because it contains three nonequivalent types of Fe atom.

Experiments on spin states under pressure probe the electron configuration only indirectly, so computational studies are necessary to resolve experimental ambiguities and to connect measurements with the correct interpretations and implications. Researchers led by Renata Wentzcovitch (University of Minnesota) have now done a computational study of Fe atoms in Pv.[1] They found that one of the three types of Fe undergoes a spin-state crossover, which has a significant effect on seismic waves and on mantle convection.

Go for a spin

Spin-state crossover arises from the behavior of electrons in a transition metal's partially filled *d* subshells. In an isolated atom, all five *d* orbitals are degenerate, but the degeneracy is lifted in the anisotropic environment of a crystal. For example, in an octahedral complex, as shown in figure 1, the two orbitals that point directly at the surrounding atoms are higher in energy than the three that point between the atoms. When that crystal-field splitting is not too great, the *d* electrons find it energetically favorable to spread out among the orbitals so their spins can align. Putting the material under pressure tends to increase the splitting; when it becomes great enough, the electrons tend instead to fill the lower-energy orbitals before occupying any of the higher-energy ones. Because the spin crossover involves the migration of electrons between distinguishable orbitals, rather than being just a spin flip, it can noticeably affect the length and strength of chemical bonds.

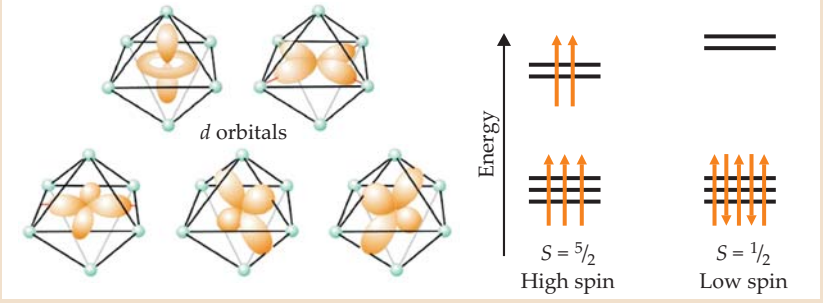

Figure 1. Spins under pressure. In a transition-metal compound, a *d* subshell is made up of two groups of orbitals with slightly different energies. The energetically favored configuration in a partially filled *d* subshell depends on the energy splitting between the two groups: When the splitting is small, electrons prefer to align their spins, even if some of them must occupy the higher-energy orbitals. But when the splitting is large, the electrons fill the lower-energy orbitals first. Compressing the material increases the splitting and thus can induce a spin-state crossover.

Iron in Pv can be either ferrous (Fe^{2+}) or ferric (Fe^{3+}). Ferrous Fe can replace Mg in the crystal structure, and ferric Fe can replace either Mg or silicon. Ferric Fe has five *d* electrons, so its spin state, as shown in figure 1, can change between $S = 5/2$ and $S = 1/2$. Ferrous Fe has six *d* electrons, so it can undergo a crossover from spin $S = 2$ to $S = 0$.

Ferrous wheel

The principal experimental techniques to study spin-state crossover are Mössbauer spectroscopy and x-ray spectroscopy on laboratory samples. Both techniques probe not the electrons but the Fe nuclear energy levels, which are affected by the electric field gradient at the nucleus and thus by the electron configuration. In 2008 two experimental groups studying ferrous Fe in Pv found a crossover between two electric field gradients that were too high to result from the low-spin, $S = 0$ configuration.[2] The experimenters thought, then, that they were seeing a crossover between high spin ($S = 2$) and intermediate spin ($S = 1$). But according to theory, such a spin-state change should be impossible.

Using techniques pioneered by Wentzcovitch, Matteo Cococcioni, and Peter Blaha, the computational team resolved the mystery.[3] The change in the electric field gradient, they found, was due not to a spin-state crossover but instead to a structural change in which an

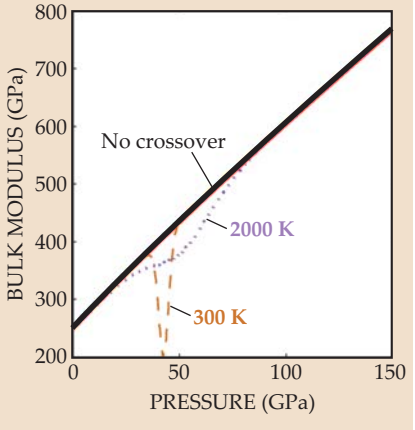

Figure 2. When a spin-state crossover is accompanied by a change in unit-cell volume, the result is a softening in the material (measured by a reduction in bulk modulus) compared to the hypothetical case of no crossover. The higher the temperature, the less prominent the softening, but the wider the range of pressures over which it occurs. (Adapted from ref. 1.)

Fe atom shifts position within a cage of surrounding oxygen atoms. The *d* electrons remain in the high-spin state all the while.

Ferric crossover

The situation with ferric Fe in Pv is more complicated because it can occupy two nonequivalent sites in the crystal lattice. Last year an experimental study, at odds with the computational studies to date and with other experiments, found that ferric Fe that replaces Si undergoes a spin-state crossover between 50 and 60 GPa (equivalent to subterranean depths of 1400–1700 km), and that ferric Fe that replaces Mg remains in the high-spin state at all pressures relevant to Earth's mantle.[4] Using the same method they'd applied to ferrous Fe, Wentzcovitch and colleagues verified that interpretation unambiguously, and they explored its geophysical consequences.[1]

The team found that for ferric Fe on the Si site, the change from $S = 5/2$ to $S = 1/2$ causes the unit cell to shrink in volume by about 1%. And the spin-state crossover isn't abrupt as a function of pressure; at nonzero temperature, there is a range of pressures over which high-spin and low-spin unit cells coexist. At those pressures, which in Earth's mantle correspond to depths from about 1000 km to 2200 km, the material is significantly more compressible than it would be in the absence of a crossover, because it's relatively easy to nudge a few more unit cells into the low-spin state. As shown in figure 2, the higher the temperature, the wider the crossover's pressure range, but the less significant the softening. In contrast, for ferric Fe on the Mg site, a change in spin causes almost no change in volume, so even if those Fe atoms did undergo spin-state crossover, it would have little effect.

Johanna Miller

References

1. H. Hsu et al., *Phys. Rev. Lett.* **106**, 118501 (2011).
2. J.-F. Lin et al., *Nat. Geosci.* **1**, 688 (2008); C. McCammon et al., *Nat. Geosci.* **1**, 684 (2008).
3. H. Hsu et al., *Earth Planet. Sci. Lett.* **294**, 19 (2010).
4. K. Catalli et al., *Earth Planet. Sci. Lett.* **289**, 68 (2010).

Atoms in a BEC engineered to have spin–orbit coupling typical of electrons in a solid

By mimicking certain electromagnetic effects, researchers can use ultracold atomic gases to simulate a wide range of many-body behavior.

Since the creation of a Bose–Einstein condensate (BEC) nearly 20 years ago, the toolbox for manipulating ultracold gases has greatly expanded. Researchers have simulated the transition from a bosonic superfluid to a Mott insulator, led fermions continuously from a molecular BEC to a Bardeen-Cooper-Schrieffer superfluid composed of widely spaced Cooper pairs, and reproduced many other phenomena seen in condensed-matter systems. And they want to do more.

Researchers envision using ultracold gases to simulate a real solid. For example, interfering laser beams can create a periodically varying potential energy in which the atoms sit, reminiscent of electrons in a crystal lattice; experimenters can adjust the depth of the potential wells or the interaction strength between the atoms. The advantage of using an ultracold atomic system is that it is much cleaner than a real solid and allows experimenters to exert much greater control over the relevant parameters.

To expand the types of simulations that can be done, however, requires the introduction of electromagnetic effects. Without such effects, there's no way to reproduce fascinating behavior like the quantum Hall effect or to further investigate semiconductor spintronics. But how can one mimic electromagnetic effects when dealing with a gas of neutral atoms?

Engineering gauge fields

One answer is to use lasers in a creative way to produce some of the same impacts on neutral atoms that a magnetic field has on charged particles.[1] About a year and a half ago, researchers from the Joint Quantum Institute (JQI) of NIST in Gaithersburg, Maryland, and the University of Maryland, College Park, used lasers to generate an effective magnetic field in a BEC (see PHYSICS TODAY, February 2010, page 17). As proof, they observed vortices that were produced while neutral atoms encircled the effective flux lines.[2]

Some of the same JQI researchers have now taken an important step further and simulated the spin–orbit coupling (SOC) between an atom's spin and its motion.[3] For electrons, SOC usually results from an electron's motion in a charge field; there's no such charge field for atoms moving in a BEC, so the JQI experimenters had to devise a way to simulate the same effect with lasers. They also found a quantum phase transition from a regime in which two spin states coexist in the same region of space to one in which they are spatially separate. The team consists of JQI researchers Yu-Ju Lin and Ian Spielman, as well as Karina Jiménez-García, of JQI and the National Polytechnic Institute of Mexico.

Jason Ho of the Ohio State University comments that the new work will open many doors for future studies. A natural extension will be to demonstrate SOC in fermions as well as bosons. In general, the SOC interaction stems from a nonabelian gauge field, although the kind simulated in the JQI work is abelian. Such fields are being widely explored for possible implementation of topological quantum computing[4] (see PHYSICS TODAY, March 2011, page 20, and the article by Sankar Das Sarma, Michael Freedman, and Chetan Nayak, July 2006, page 32).

Patrik Öhberg of Heriot-Watt University in Edinburgh, UK, notes that the new SOC technique allows experimenters to adjust parameters, such as the coupling strength, that otherwise are set by nature. In addition, it has resulted in a new type of particle—a boson with SOC—that has not been studied before. In certain circumstances, he says, such a condensate "might mimic relativistic dynamics, even if it is ultracold."

Artificial fields

In atomic physics, SOC is an interaction between an electron's spin and its motion about the nucleus; for solids, it's the link between the electron's spin and its motion in the charge field of the underlying lattice. Taking a broader view of SOC, Spielman explains, his group sought a way to link the internal spin of an atom to its momentum. They did that with a pair of laser beams. He and his colleagues started with a BEC of rubidium-87 atoms. In place of an electron's two spin states—up and down—they focused on two particular hyperfine states of the ^{87}Rb atom's $5S_{1/2}$ $F = 1$ electronic ground state, referring to them as pseudospin states. The hyperfine state with $m_F = 0$ was taken to be the